RSC Advances

ROYAL SOCIETY OF CHEMISTRY

www.rsc.org/advances

Table of Content

Reduced Graphene Oxide can be used as sensor transducer in Field Effect Transistor (FET) biosensors for sensitive and label-free detection of Interleukin-6 proteins, by overcoming the (1) variable coverage and (2) high electrical resistance, via ethanol Chemical Vapour Deposition (CVD).

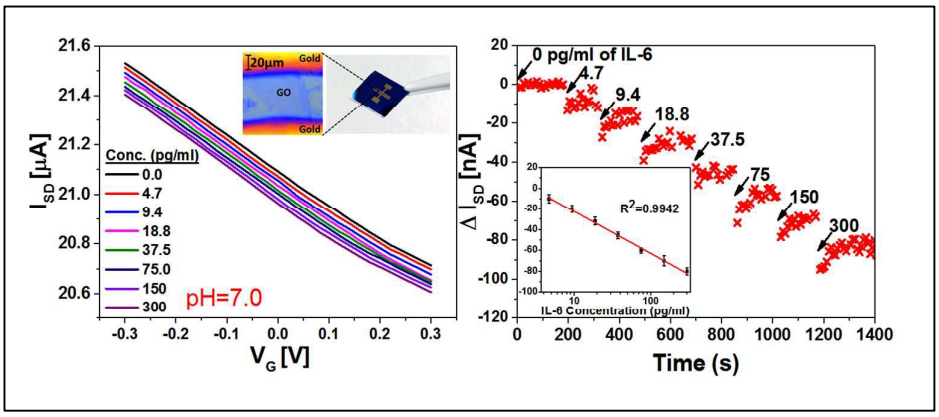

RSC Advances

RSCPublishing

ARTICLE

Highly Manufacturable Graphene Oxide Biosensor for Sensitive Interleukin-6 Detection

Cite this: DOI: 10.1039/xoxxoooooox

Jingfeng Huang,[a,b,c] Hu Chen,[a,b] Wenbin Niu,[a] Derrick W.H. Fam,[d] Alagappan Palaniappan,[a,e] Melanie Larisika,[f,e] Steve H. Faulkner,[c] Christoph Nowak,[f,e], Myra A. Nimmo[b,c,g] ,Bo Liedberg,[*a,e] and Alfred I.Y. Tok[*a,b]

Received ooth January 2015,
Accepted ooth January 2015

DOI: 10.1039/xoxxoooooox

www.rsc.org/

Graphene Oxide (GO) is analogous to graphene with oxygen moieties. It offers several advantages over graphene, such as a tunable band-gap, facile synthesis and without the use of metal catalysts. Due to the monolayer configuration of GO, all of its carbon atoms are readily exposed to the atmosphere and are sensitive to surface perturbations, thus making GO very suitable for liquid-gated field effect transistor (FET) type sensing applications. However, there are two main limitations preventing GO usage in practical FET sensors. It displays (1) variable coverage between fabricated chips and (2) high electrical resistance. In this paper, we overcome these two limitations by using a facile atmospheric-pressure ethanol Chemical Vapor Deposition treatment on top of pre-coated GO (ECVDGO) which decreases the electrical resistivity from $1.99x10^6$ Ω/square to $4.68x10^3$ Ω/square, and resistivity variation from $1.60x10^6$ to $7.72x10^2$ Ω/square; whilst enlarging the surface GO coverage up to 100%. We then demonstrate the ability of the post-treated ECVDGO liquid-gated FET transducer to detect Interleukin-6 which is a multi-functional cytokine involved in regulating the immune function and the acute phase response. The sensing window of the fabricated biosensor to Interleukin-6 is within physiological-relevant range, from 4.7 to 300pg/ml. The LOD of the sensor based on 3σ is 2.9pA or 1.53pg/ml. This study demonstrates the emerging potential of GO with high manufacturability in liquid-gated FET biosensors for sensitive and label-free detection of bio-molecules.

1. Introduction

Interleukin-6 (IL-6) is an important human pleiotropic cytokine, which is reported to have both pro- and anti-inflammatory effects.[1, 2] It is involved in extensive biological activities such as the regulation of immune system and the acute phase response. During acute exercise, IL-6 is released from the working skeletal muscle and the corresponding level increases as a function of the intensity and duration of the exercise. This change is not linear, but follows a near-exponential pattern. Plasma IL-6 concentrations have been reported to increase by more than 100-fold in response to prolonged exercise,[3] with IL-6 peaking at the cessation of exercise, or shortly thereafter and it is followed by a rapid decrease to baseline levels.[4] Protracted high IL-6 levels could also indicate cancer and other chronic diseases.

Furthermore, it had been reported recently that there is no difference in the measurement of plasma IL-6 using the more invasive venous versus the minimally invasive capillary blood sampling measurement.[5] The possible use of capillary measurement meant a minimally invasive way to quantitatively monitor changes in plasma IL-6 levels. The use of capillary sampling is also a more accessible, tolerable and faster way for field-based blood measures, for example, during sport providing an ideal route for point-of-care testing. Thus the IL-6 protein has immense potential as a training and fatigue biomarker if it can be measured in real-time.

Table 1 Comparison of recently reported biosensors to IL-6.

Reference	Transducer	Platform	Sensitivity range (pg/ml)	Note
Reported	Post-processed Graphene Oxide	FET immunoassay	4.7-300	Label-free
[6]	Microfabricated silicon flexural plate wave (FPW) resonators	Micro-electromechanical (MEM) immunoassay	1.2-unknown	Label-free
[7]	Fiber-optic dip-probe	Optical immunoassay	120-12000	Label-free
[8]	Functionalized Biacore sensor chip	Surface plasmon resonance (SPR) immunoassay	780 to 12500	Label-free
[9]	SWCNTs/AuNPs	Electrochemical impedance immunoassay	$1e^{-5}$ – 0.1	AuNPs
[10]	Polymeric nanoparticles on calcium carbonate	Electrochemical immunoassay	2-20000	Porous polyelectrolyte nanoparticles label used
[11]	Modified carbon electrodes	Electrochemical immunoassay	0.01-$1e^{6}$	PS@PDA-metal label used
[12]	Carbon Nanotube Forest Electrodes	Electrochemical immunoassay	0.5−30	Ab2-MWNT-HRP label used
[13]	Functionalized fluorescent core-shell nanoparticles	Fluoro- immunoassay	20-1250	Fluorescent core-shell nanoparticles label used

Currently, ELISA and western blotting are the gold standards for IL-6 detection.[14] These techniques require substantial time, cost, machinery and specialist training; thus making real-time detection of IL-6 impossible. In contrast, a liquid-gated FET biosensor offers real-time monitoring and requires only a single antibody to capture the antigen and report a signal. When the target antigen binds to the antibody, it changes the environment near the surface of the transducer and alters its electrical conductance.[15] Table 1 compares the sensitivity range of different types of biosensors to IL-6 reported recently. Although the sensitivity range of electrochemical immunoassay[11] with modified carbon electrodes is much wider than that of the FET immunoassay reported in this work, it is noted that most electrochemical immunoassays require secondary markers or antibody labels as reporter molecule which involves additional costs and processing time.[9,10,11,12] Using the reported real-time label-free graphene oxide sensor, the sensitivity range is within the physiological range of ~10pg/ml in sweat samples from healthy women[16, 17] which were not to be significantly different from plasma levels ($p=0.19$;[16]).

Graphene oxide (GO) is analogous to graphene with oxygen moieties and has the distinct advantages of being solution processable, industrially scalable and a tunable electronic band-gap.[18, 19] Due to the monolayer configuration of GO, all its carbon atoms are exposed to the environment and the charge-carriers are confined to the surface of the sheets. Thus the electrical conductivity of the flake is very sensitive to local electrostatic perturbations.[20] This property makes it suitable for sensing applications. GO biosensors have been reported for the detection/discrimination of antibody oxytetracycline (4pg/ml-1μg/ml),[21] antibody Immunoglobin E (1pM-10nM),[22] bacterium Vibrio cholera (0.12nM-5.4nM),[23] nucleic acid DNA (1.0fM-0.1μM),[24] tumour marker carcinoembryonic antigen (0.1pg/ml-20ng/ml)[25] and monoamine catecholamine (1mM-10mM).[26]

There are however, inherent limitations in GO that prevent it from being used as an ultra-sensitive and high-loading transducer in FET molecular sensing applications. These limitations need to be resolved before GO can be used in practical applications. For example, the coverage of GO on SiO_2 substrate ranges from ca. 60-90% due to the inefficient self-assembly of GO flakes and undesirable cross-linking within the 3-AminoPropylTriEthoxy Silane (APTES) adhesion layer. APTES is commonly used in literature [26-29] to form a positively-charged surface for the negatively-charged GO to self-assemble via electrostatic attraction. This incomplete coverage leads to variable available sensor surface area, and more importantly, high sheet resistance that limits the sensitivity of the biosensor.[26]

Various GO pre- and post-treatment such as ultrasonication to obtain larger GO sheets,[29, 30] short ethanol Chemical Vapor Deposition (CVD) treatment to obtain increased graphitization [31] and hydrogen heat treatment to obtain improved reduction [32] have been reported. However, none of these strategies can produce a combination of these solutions.

In this paper, we demonstrate a post-treatment of GO using atmospheric ethanol CVD which can increase the size, graphitization and reduction of GO and thus removing limitations of high electrical resistance and variability to yield a practical liquid-gated FET transducer platform suitable for real-time and sensitive detection of molecules. The ethanol CVD post-treated GO is termed ECVDGO. We then determine the

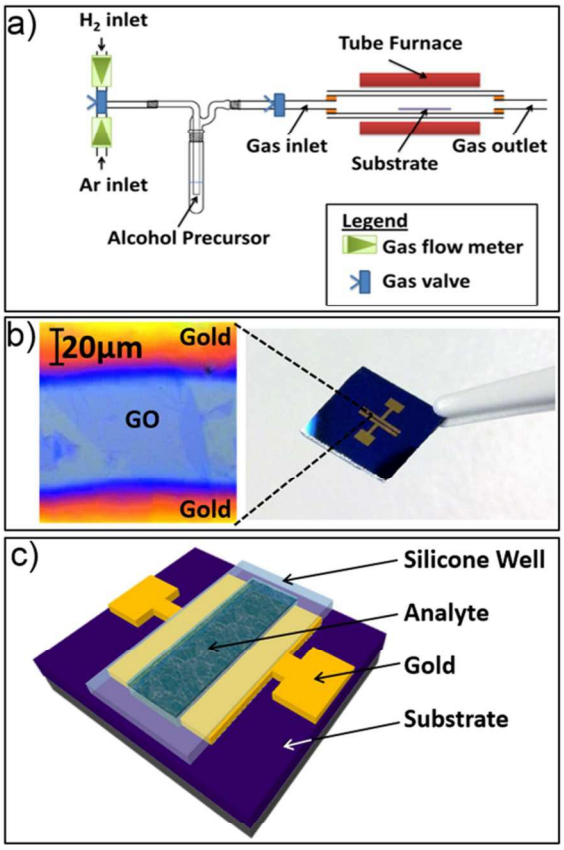

Figure 1 (a) Schematic illustration of the ethanol CVD tube furnace setup; (b) microscope image and photograph of fabricated gold electrode on GO; and (c) schematic illustration of fabricated biosensor chip with silicone well and analyte.

sensing characteristics and window of the sensor to IL-6 proteins.

2. Experimental Procedure

2.1. Preparation of large GO flakes on silicon substrates

A modified Hummers method[29, 30, 33] was used to obtain large sized GO. Briefly, 2 g of graphite (3.5mm flakes, NGS) was stirred with concentrated H_2SO_4 (12 ml) for 4 hours at 80 °C. The mixture was cooled to room temperature and ultrasonicated for 1 hour. Water (500 ml) was then added and the mixture was left overnight. The next day, it was washed over a 0.2 µm filter. The product was dried and stirred with concentrated H_2SO_4 (120 ml) and $KMnO_4$ (15 g). After 2 hours, the solution was diluted with water (250 ml) in an ice bath. After another 2 hours, water (700 ml) and H_2O_2 (20 ml) was added. The obtained mixture was dialyzed and centrifuged to obtain GO stock solution.

Standard procedure involving RCA cleaning of SiO_2 substrates was employed. The substrates were then immersed in 1 % v/v (3-Aminopropyl) triethoxysilane absolute-ethanol solution for 1 h in a dry box followed by rinsing thoroughly with ethanol to remove physisorbed APTES. The substrates were then baked in an oven for 1 h at 120 °C to introduce crosslinking.[34] The prepared GO solution was drop-casted on the substrates and left to stand for 1 hour. APTES covalently attaches to the hydroxyl groups of the freshly cleaned SiO_2 surface and modifies the surface with $-NH^{3+}$ groups to become positively charged[34]. The GO, which is negatively charged in aqueous media of low to medium pH, then electrostatically attaches to the surface. Finally, the prepared substrates with 1-2 layers of GO were rinsed, blow-dried and kept in desiccator.

2.2. Ethanol CVD post-treatment of GO substrate

The prepared substrates were placed in the middle of an ethanol CVD tube furnace setup (Figure 1a). The tube was purged with 300 sccm of Ar gas for 30 mins. The flow was then adjusted to 100 sccm and 20 sccm for Ar and H_2 respectively. Subsequently, the gases were passed through the ethanol column and the furnace set to 950 °C at 40 °C per second ramp. After 2 hours, the ethanol valves and furnace were turned off and left to cool slowly to ambient temperature.

2.3. Fabrication of liquid-gated FET sensor

Gold electrodes of 100 nm thickness with a titanium adhesive layer of 20 nm thickness were thermally-evaporated on the surface of the substrate using shadow mask. The channel dimension is 100µm by 4 mm (Figure 1b). The surrounding ECVDGO around the electrodes were scraped off the surface using a metal tweezers wrapped with IPA soaked clean-room cloth. The remaining ECVDGO layer is however stable under normal test conditions. The electrical resistance in liquid was stable for more than 4 hours. Two dots of silver paint (RS186-3600) were dropped onto the gold electrodes and dried at 120°C for 10 mins to protect the fabricated gold electrodes from measuring probe scratches. A silicone gel well was then fabricated onto the electrodes to hold the liquid test analyte (Figure 1c).

Then 30µl of 6mM 1-pyrenebutanoic acid, succinimidyl ester (PBSE) linker molecules with DMF were placed into the well for 1 hour and then rinsed thoroughly. IL-6 antibody were subsequently incubated on the surface for 2 hour and rinsed. The ECVDGO sensor was then blocked with bovine serum albumin and ethanolamine in fetal bovine serum to prevent non-specific interferences. The chips were kept under moist conditions at 4°C before measurement.

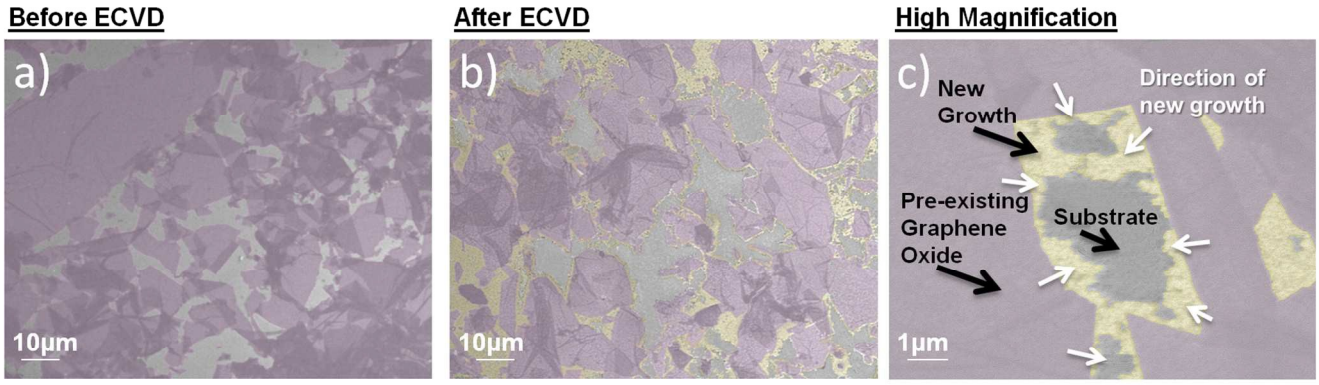

Figure 2: Scanning electron microscope of (a) before and (b) after ethanol CVD growth GO flakes. The coverage increased from 60 to 80% after a 30 minutes treatment. The pre-existing graphene oxide flakes are highlighted in purple and the growths are highlighted in yellow. (c) High magnification of the growth which start growing from edges of existing flakes.

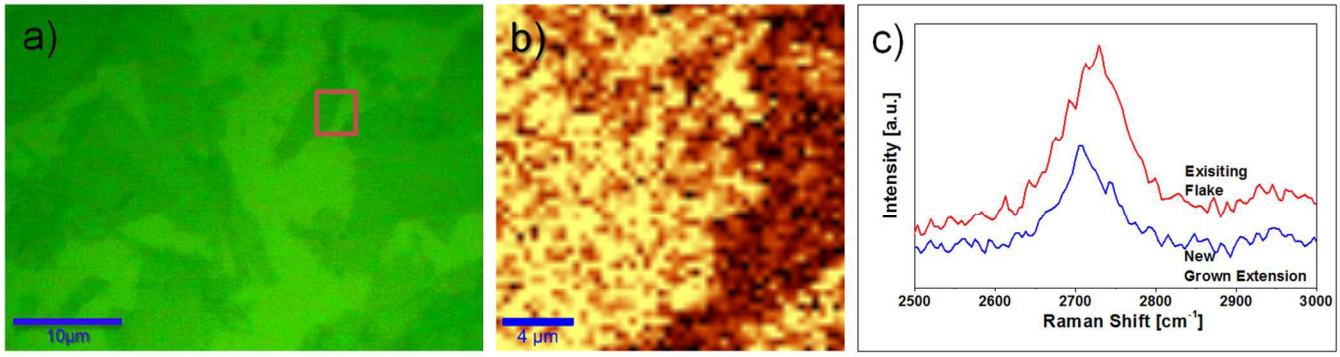

Figure 3: (a) Microscope image of ECVDGO after 2 hours with a red square indicating region where Raman mapping is performed; (b) Raman mapping showing complete GO coverage of the substrate; and (c) the 2D Raman spectrum used to distinguish the contrast in the Raman mapping.

2.4. Measurement of IL-6

A liquid gate potential is applied (4200-SCS, Keithley) to a well-defined and stable reference electrode (Ag/AgCl, 3M KCl, WPI) with respect to the grounded drain electrode. Small source drain bias voltage of 10mV was applied across the FET channel to monitor the device resistance. PBS buffer was added to the chip to obtain a baseline. Then, different concentrations of proteins were added to get different device current-voltage curves. 1x PBS concentration was used as it is similar to biological conditions and prevents the solution gating operations to shift positively which is unfavorable for solution gating operations[35]. Immunoglobulin Isotype-G (IGG) purified monoclonal recombinant antibodies comprising of two heavy and two light chains to IL-6 (555220 kit, BD) and recombinant human IL-6 proteins (555220 kit, BD) were used.

3. Results and Discussions

Due to the undesirable cross-linking within the 3-AminoPropylTriEthoxy Silane (APTES) adhesion layer[36] and the intrinsic inefficient self-assembly of GO flakes, the coverage of GO ranges variably from ca. 60-90%. The electrical conductivity is thus decreased and the standard deviation between chips is increased. The variable coverage also prevents the manufacturability and reproducibility of GO substrates for any applications. Figure 2a shows a SEM image of the substrate before growth with an initial coverage of ca. 60%.

After a partial 30-minute treatment with the ethanol CVD, the coverage can be increased from 60 to 80%. The growths are highlighted in yellow in Figure 2b. Figure 2c shows a higher magnification SEM image that indicate that the growth extension starts from the edges of existing flakes and continues outwards into the empty gaps between flakes. The new growth also covers existing flakes. As the ethanol CVD treatment continues to 2 hours, the new growths cover all the gaps between pre-existing new gaps completely.

Raman spectroscopy (488nm) was used to confirm the complete coverage of the 2 hours ethanol CVD treated samples. A contrast between the existing flakes and new growth extensions can be observed in the microscope image in Figure

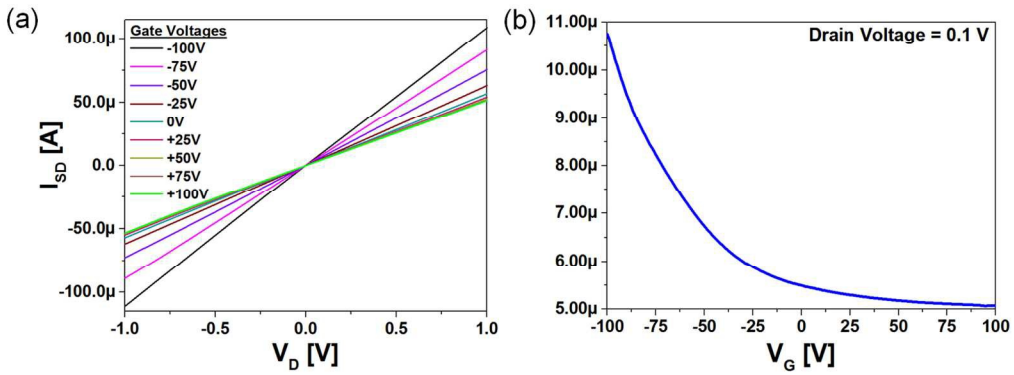

Figure 4 The back-gated ECVDGO FET (a) output characteristic drain current-drain voltage (I_{SD}-V_D) curve under different applied gate voltages; and (b) corresponding transfer (I_{SD}-V_G) curve under fixed drain voltage, V_D=0.1V. Both measured under ambient conditions.

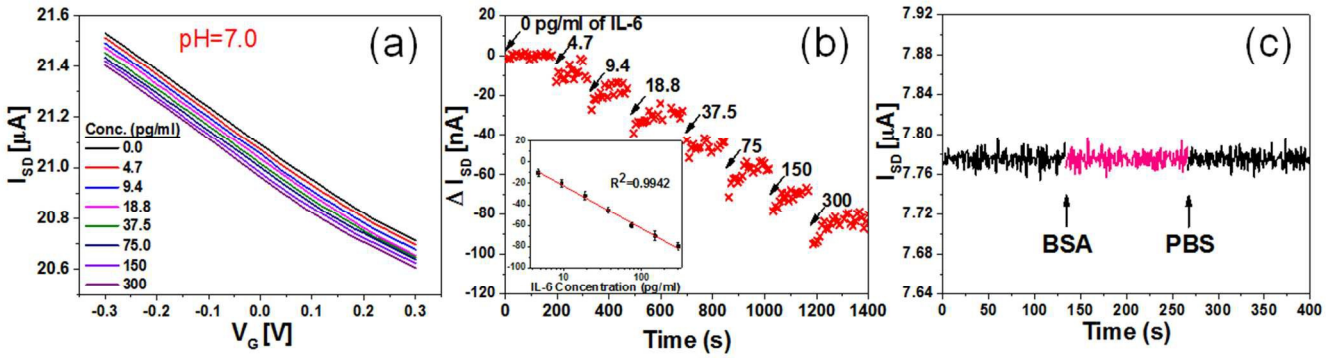

Figure 5: Detection characteristics of liquid-gated ECVDGO FET biosensors. (a) Source-drain current [I_{sd}] vs. gate voltage [V_G] plot with different concentration of IL-6 protein, showing decreasing I_{SD} at increasing IL-6 addition; (b) I_{SD} vs. time with addition of 0-300pg/ml of IL-6; and (c) real-time I_{SD} plot, showing negligible effect when BSA interference protein was added.

3a. This contrast is due to the thickness difference between the new growth and pre-existing flakes on SiO_2[37], where the darker contrast area indicates thicker layer. The presence of new growth extensions was confirmed in the Raman mapping shown in Figure 3b. The 2D Raman spectrum (23cm^{-1} difference) was used to distinguish the existing flakes from the new growth extension because the former has an upshifted position that is due to increased number of graphene layers[19, 38]

To quantify the improvement in electrical conductivity, 5 samples of 2-hour ECVDGO and hydrazine-reduced GO[29] were measured under the 4-point probe setup. All the chips were made in a single batch for accurate comparison. The measured electrical resistance of the ECVDGO sample decreased from $1.99x10^6$ to $4.68x10^3$ Ω/square compared to hydrazine reduced samples, whilst the relative standard deviation of ECVDGO samples decreased from 80.4% to 16.5%. Thus the ethanol CVD post-processing treatment reduced the electrical variability of GO across the samples and also improved the electrical conductivity.

The ECVDGO samples were then fabricated into back-gated transistor to measure the transfer characteristic transistor output under ambient temperature and pressure. Channel length of 100µm was fabricated to ensure bulk-limiting transport behaviour and decrease the role of contacts. The linear output behaviour of the back-gated device (Figure 4a) at various gate voltages shows good ohmic contact between the transducer and the electrodes. The device is stable in large gate voltages (V_g) ranging from -100V to +100V. The corresponding transfer curve (I_{SD}-V_G) of the transistor under drain bias voltage, V_D = 0.1V, is shown in Figure 4b. The current of the transfer curve are much higher at negative gate voltages compared to positive voltages. These indicate that the holes are the main charge carriers of ECVDGO under ambient condition.

The ECVDGO material was then used to fabricate liquid gated transistors for IL-6 sensing application and the shift in source-drain current (I_{SD}) of the anti-IL-6 immobilized ECVDGO transistor is sensitive to increasing concentrations of IL-6 protein due to electronic n-doping of the device. Figure 5a shows that binding of increasing amounts of IL-6 protein to the anti-IL-6 antibody results in a down-shift of the I_{SD}-V_G curve, from 21.09µA (0pg/ml) to 20.96 µA (300pg/ml) at V_G=0V.

Low gate voltages were used to minimize possible disturbances to the biological sample and prevent instability of the biosensor due to electrochemical and charging effect.[26] The sensor was

operating in the p-type region at V_G=0V and the negative shift is tentatively attributed to the electrostatic gating effect on the ECVDGO surface.

Increasing density of overall positive charges from the immune-complex induces negative charges in the ECVDGO. This n-doping shifts the transconductance curve to more negative gate volatges.[15, 39] Additionally, responses could also be due to a decreased ionic screening effect after the protein-antibody interaction.[40-42] The decrease in I_{SD} corresponds to a sensitivity of 1.5pA per pg/ml of IL-6. The slope of the I_{SD}-V_G curve does not change thus indicating that the charge carrier mobility in the ECVDGO transducer remains the same after the protein-antibody reaction. It is noted that I_{SD} downshift (electrostatic gating effect) exhibited in our biosensor is more reproducible and reliable than other effects using Schottky barrier and changes in gate coupling and carrier mobility.[15]

The change in I_{SD} can then be utilized to be a sensor for the IL-6 concentration by fixing the gate voltage value. The general trend of the I_{SD} decreasing with increasing concentration of IL-6 is evident in the calibration curve (Figure 5b). The linear dynamic range (LDR) of the sensor is from 4.7 to 18.8 pg/ml of IL-6. Although at higher concentrations, the change in the sensor electrical signal was not much higher than at 18.8pg/ml, but the sensor still acts as an active material that gave a reliable reading against IL-6 concentrations (Figure 5b insert). The slightly non-linear relationship between interleukin-6 concentration and the decrease of measured source-drain current could be attributed to the carrier injection during the I-V measurement.[43] It has also been commonly observed for carbon-based FET biosensors.[26, 43-46] Further studies are needed to reveal the details of the sensing mechanisms. Figure 5c shows no change in the I_{SD} when the sensor is exposed to interference protein, BSA. This shows the sensor resistance (after IL-6 attachment and blocking agent protection) in preventing interferences and unspecific binding.

The LOD of the ECVDGO sensor based on 3σ is 2.9pA (equivalent to 1.53pg/ml). Plasma IL-6 levels in physically active individuals have been reported to be as low as ≤1pg/ml[3, 47] while levels in sedentary middle-aged men ~11pg/ml and healthy premenopausal women have been reported in the range of ~10-11pg/ml.[16] Following prolonged exercise such as cycling, IL-6 can be elevated as much as 38 fold, and as much as 128 fold following completion of a marathon;[3] therefore the detection range of the reported sensor is within the physiological range of IL-6.

The eventual end point application would be for point of care and whole blood analysis. Thus the ability of the ECVDGO sensor to sensitively and selectively detect the biomarker in serum demonstrates its relevance to potential usage in medical diagnostics. Future work from the results of this experiment could be used to develop portable, real-time, low-cost and robust amperometric biomarkers detection array, kinetic study platform for the study of liposomes[48] and synthetic aptamers.

4. Conclusions

Two important factors for high manufacturability of biosensors are the homogeneity and also the sensitivity of the transducer. Herein, we devised an ethanol CVD post-treatment of 2 hours on pre-coated GO substrates to form a complete coverage achieving significantly lower electrical resistivity (~$4.68x10^3$ Ω/square) and deviation (~$7.72x10^2$ Ω/square) as compared to typical hydrazine reduced GO. We then demonstrated that the ECVDGO act as a sensitive active material for IL-6 measurement within the human physiological range of 4.7-300pg/ml. The LOD of the sensor based on 3σ is 2.9pA or 1.53pg/ml. The specificity of the biosensor to IL-6 was also demonstrated. This study highlights the emerging potential of post-treated GO based biosensors in sensitive and label-free detection of bio-molecules, particularly, in detection for interleukin based proteins which have been reported to be linked to diagnostic of fatigue and inflammatory.

Acknowledgements

The author is grateful for the research funding from the Institute for Sports Research (ISR) of Nanyang Technological University (NTU). The research was also partly supported by the National Institute for Health Research (NIHR) Diet, Lifestyle & Physical Activity Biomedical Research Unit based at University Hospitals of Leicester and Loughborough University. The views expressed are those of the authors and not necessarily those of the NHS, the NIHR or the Department of Health.

Notes

[a] School of Materials Science and Engineering, Nanyang Technological University, Singapore 639798. Tel.: +65 67904935. E-mail address: miytok@ntu.edu.sg.
[b] Institute for Sports Research, Nanyang Technological University, 50 Nanyang Avenue, Singapore 639798.
[c] School of Sport, Exercise and Health Sciences, Loughborough University, Leicestershire, UK, LE113TU.
[d] Department of Chemistry, Royal College of Science, Imperial College, Exhibition Road, London, UK, SW72AZ.
[e] Centre for Biomimetic Sensor Science, Nanyang Technological University, Singapore 637553.
[f] Austrian Institute of Technology (AIT) GmbH, Donau-City Str.1, Vienna, Austria 1220.
[g] The University of Birmingham, College of Life and Environmental Sciences, Birmingham, UK, B15 2TT.

References

1. M. Leggate, M. A. Nowell, S. A. Jones and M. A. Nimmo, *Cell stress & chaperones*, 2010, **15**, 827-833.
2. J. Scheller, A. Chalaris, D. Schmidt-Arras and S. Rose-John, *Biochimica et Biophysica Acta (BBA) - Molecular Cell Research*, 2011, **1813**, 878-888.
3. K. Ostrowski, T. Rohde, S. Asp, P. Schjerling and B. K. Pedersen, *The Journal of physiology*, 1999, **515**, 287-291.
4. K. Ostrowski, T. Rohde, M. Zacho, S. Asp and B. K. Pedersen, *The Journal of physiology*, 1998, **508**, 949-953.
5. S. Faulkner, K. Spilsbury, J. Harvey, A. Jackson, J. Huang, M. Platt, A. Tok and M. Nimmo, *Eur J Appl Physiol*, 2014, **114**, 1207-1216.

6. J. Pepper, R. Noring, M. Klempner, B. Cunningham, A. Petrovich, R. Bousquet, C. Clapp, J. Brady and B. Hugh, *Sensors and Actuators B: Chemical*, 2003, **96**, 565-575.
7. R. Kapoor and C.-W. Wang, *Biosensors and Bioelectronics*, 2009, **24**, 2696-2701.
8. T.-H. Chou, C.-Y. Chuang and C.-M. Wu, *Cytokine*, 2010, **51**, 107-111.
9. T. Yang, S. Wang, H. Jin, W. Bao, S. Huang and J. Wang, *Sensors and Actuators B: Chemical*, 2013, **178**, 310-315.
10. T. Li and M. Yang, *Sensors and Actuators B: Chemical*, 2011, **158**, 361-365.
11. J.-J. Shi, T.-T. He, F. Jiang, E. S. Abdel-Halim and J.-J. Zhu, *Biosensors and Bioelectronics*, 2014, **55**, 51-56.
12. R. Malhotra, V. Patel, J. P. Vaqué, J. S. Gutkind and J. F. Rusling, *Analytical Chemistry*, 2010, **82**, 3118-3123.
13. X. Hun and Z. Zhang, *Biosensors and Bioelectronics*, 2007, **22**, 2743-2748.
14. S. R. Gray, M. Robinson and M. A. Nimmo, *Cell stress & chaperones*, 2008, **13**, 247-251.
15. I. Heller, A. M. Janssens, J. Männik, E. D. Minot, S. G. Lemay and C. Dekker, *Nano Letters*, 2007, **8**, 591-595.
16. A. Marques-Deak, G. Cizza, F. Eskandari, S. Torvik, I. C. Christie, E. M. Sternberg and T. M. Phillips, *Journal of immunological methods*, 2006, **315**, 99-109.
17. G. Cizza, A. H. Marques, F. Eskandari, I. C. Christie, S. Torvik, M. N. Silverman, T. M. Phillips and E. M. Sternberg, *Biological psychiatry*, 2008, **64**, 907-911.
18. J. Huang, M. Larisika, C. Nowak and I. Y. A. Tok, *New Methods in Aqueous Graphene (Graphene Oxide) Synthesis for Biosensor Devices*, Taylor & Francis Group, Oxford, UK, 2014.
19. J. Huang, D. Fam, Q. He, H. Chen, D. Zhan, S. H. Faulkner, M. A. Nimmo and A. I. Yoong Tok, *Journal of Materials Chemistry C*, 2014, **2**, 109-114.
20. J. Huang, J. Harvey, H. Chen, M. A. Nimmo and I. Y. A. Tok, Conference Proceeding of icSports, Vilamoura, Portugal, 2013.
21. W. Xu, S. Liu, J. Yu, M. Cui, J. Li, Y. Guo, H. Wang and J. Huang, *RSC Advances*, 2014, **4**, 10273-10279.
22. K.-J. Huang, Y.-J. Liu, J.-T. Cao and H.-B. Wang, *RSC Advances*, 2014, **4**, 36742-36748.
23. P. R. Solanki, S. Srivastava, M. A. Ali, R. K. Srivastava, A. Srivastava and B. D. Malhotra, *RSC Advances*, 2014, **4**, 60386-60396.
24. Z. Zhang, L. Luo, G. Chen, Y. Ding, D. Deng and C. Fan, *Biosensors and Bioelectronics*, 2014, **60**, 161-166.
25. Y. He, Y. Chai, H. Wang, L. Bai and R. Yuan, *RSC Advances*, 2014, **4**, 56756-56761.
26. Q. He, H. G. Sudibya, Z. Yin, S. Wu, H. Li, F. Boey, W. Huang, P. Chen and H. Zhang, *ACS Nano*, 2010, **4**, 3201-3208.
27. Z. Wang, J. Zhang, P. Chen, X. Zhou, Y. Yang, S. Wu, L. Niu, Y. Han, L. Wang, P. Chen, F. Boey, Q. Zhang, B. Liedberg and H. Zhang, *Biosensors and Bioelectronics*, 2011, **26**, 3881-3886.
28. M. Veerapandian, Y.-T. Seo, K. Yun and M.-H. Lee, *Biosensors and Bioelectronics*, 2014, **58**, 200-204.
29. M. Larisika, J. Huang, A. Tok, W. Knoll and C. Nowak, *Materials Chemistry and Physics*, 2012, **136**, 304-308.
30. C.-Y. Su, Y. Xu, W. Zhang, J. Zhao, X. Tang, C.-H. Tsai and L.-J. Li, *Chemistry of Materials*, 2009, **21**, 5674-5680.
31. C.-Y. Su, Y. Xu, W. Zhang, J. Zhao, A. Liu, X. Tang, C.-H. Tsai, Y. Huang and L.-J. Li, *ACS Nano*, 2010, **4**, 5285-5292.
32. A. Bagri, C. Mattevi, M. Acik, Y. J. Chabal, M. Chhowalla and V. B. Shenoy, *Nat Chem*, 2010, **2**, 581-587.
33. J. Huang, M. Larisika, W. H. D. Fam, Q. He, M. A. Nimmo, C. Nowak and I. Y. A. Tok, *Nanoscale*, 2013, **5**, 2945-2951.
34. M. Zhu, M. Z. Lerum and W. Chen, *Langmuir*, 2012, **28**, 416-423.
35. R. Jones and H. Meixner, *Sensors, Micro- and Nanosensor Technology: Trends in Sensor Markets*, Wiley, 2008.
36. G.-J. Zhang, T. Tanii, T. Funatsu and I. Ohdomari, *Chemical Communications*, 2004, 786-787.
37. Z. H. Ni, H. M. Wang, J. Kasim, H. M. Fan, T. Yu, Y. H. Wu, Y. P. Feng and Z. X. Shen, *Nano Letters*, 2007, **7**, 2758-2763.
38. G. Eda, G. Fanchini and M. Chhowalla, *Nat Nano*, 2008, **3**, 270-274.
39. I.-Y. Sohn, D.-J. Kim, J.-H. Jung, O. J. Yoon, T. Nguyen Thanh, T. Tran Quang and N.-E. Lee, *Biosensors and Bioelectronics*, 2013, **45**, 70-76.
40. F. Chen, J. Xia and N. Tao, *Nano Letters*, 2009, **9**, 1621-1625.
41. F. Chen, Q. Qing, J. Xia, J. Li and N. Tao, *Journal of the American Chemical Society*, 2009, **131**, 9908-9909.
42. D.-J. Kim, I. Y. Sohn, J.-H. Jung, O. J. Yoon, N. E. Lee and J.-S. Park, *Biosensors and Bioelectronics*, 2013, **41**, 621-626.
43. S. Mao, G. Lu, K. Yu, Z. Bo and J. Chen, *Advanced Materials*, 2010, **22**, 3521-3526.
44. J. P. Kim, B. Y. Lee, J. Lee, S. Hong and S. J. Sim, *Biosensors and Bioelectronics*, 2009, **24**, 3372-3378.
45. M. Abe, K. Murata, A. Kojima, Y. Ifuku, M. Shimizu, T. Ataka and K. Matsumoto, *The Journal of Physical Chemistry C*, 2007, **111**, 8667-8670.
46. T. Yang, S. Wang, H. Jin, W. Bao, S. Huang and J. Wang, *Sensors and Actuators B: Chemical*, 2013, **178**, 310-315.
47. H. Bruunsgaard, H. Galbo, J. Halkjaer-Kristensen, T. L. Johansen, D. A. MacLean and B. K. Pedersen, *The Journal of physiology*, 1997, **499 (Pt 3)**, 833-841.
48. H. Chen, S. K. Lim, P. Chen, J. Huang, Y. Wang, A. Palaniappan, M. Platt, B. Liedberg and A. I. Y. Tok, *Physical Chemistry Chemical Physics*, 2015, **17**, 3451-3456.